Low-energy electron-impact dissociative excitation of molecular hydrogen and its isotopologues

Liam H. Scarlett,[1,*] Jonathan K. Tapley,[2] Dmitry V. Fursa,[1] Mark C. Zammit,[3,1] Jeremy S. Savage,[1] and Igor Bray[1]

[1]*Curtin Institute for Computation and Department of Physics, Astronomy and Medical Radiation Sciences, Curtin University, Perth, Western Australia 6102, Australia*

[2]*School of Physics, The University of Western Australia, Crawley, Western Australia 6009, Australia*

[3]*Theoretical Division, Los Alamos National Laboratory, Los Alamos, New Mexico 87545, USA*

(Received 9 September 2017; published 21 December 2017)

We apply the adiabatic nuclei convergent close-coupling method to electron-impact dissociative excitation of H_2 in the low-energy regime. Differential and integrated cross sections are presented for excitation of the $b^3\Sigma_u^+$ state, the primary pathway to dissociation of H_2 at low energies. Agreement with experiment is satisfactory. Results are also presented for the isotopologues D_2, T_2, HD, HT, and DT, which show a pronounced isotope effect near threshold in both the differential and integrated cross sections.

DOI: 10.1103/PhysRevA.96.062708

I. INTRODUCTION

Electron-impact dissociative excitation of H_2 plays an important role in astrophysics, atmospheric physics, and plasma modeling. Electron interactions with H_2 contribute to the heating and cooling of the Jovian and Saturnian atmospheres, and play important roles in the cooling of molecular clouds, a mechanism for stellar formation [1,2]. The same processes also contributed to the energy loss of plasma electrons during the formation of the interstellar medium [3]. Molecules such as H_2 can form in the divertor region of tokamak reactors, where external cooling results in a steep temperature gradient. Collisionally induced dissociation of H_2 is a major factor governing the dynamics and properties of the plasma edge, which in turn affects the performance of the core plasma [4].

At low energies, the primary pathway to dissociation of H_2 is through excitation of the $b^3\Sigma_u^+$ state. This is a purely dissociative state and produces neutral fragments $H(1s) + H(1s)$ with considerable kinetic energies [5]. Measurements of the $b^3\Sigma_u^+$ excitation integrated cross sections (ICS) and differential cross sections (DCS) are available at incident energies of 9.2 eV and above; see Nishimura and Danjo [6], Khakoo and Segura [7], and Hall and Andric [8]. The review of Yoon *et al.* [9] provided a recommended ICS that follows these measurements. Agreement between the measurements is reasonable up to about 15 eV, although the experimental uncertainties are relatively large. The recommended cross section follows the measurements of Khakoo and Segura [7] up to 20 eV; however, there is disagreement at the cross-section peak between this experiment and the measurements of Nishimura and Danjo [6], which are significantly lower.

A large number of calculations of the $b^3\Sigma_u^+$ excitation have previously been performed in the fixed-nuclei (FN) approximation; see, for example, the calculations by Schneider and Collins [10], da Costa *et al.* [11], Branchett *et al.* [12], Gorfinkiel and Tennyson [13], Fliflet and McKoy [14], and earlier calculations referenced therein. These calculations are all in significant disagreement with each other and with the recommended data [9].

Recently, Zammit *et al.* [15] provided a comprehensive set of accurate excitation, ionization, and grand total cross sections for e^--H_2 scattering, obtained using the single-center molecular convergent close-coupling (CCC) method. These calculations were performed in the FN approximation, with the internuclear distance fixed at the mean separation $R_m = 1.448a_0$ of the ground vibrational state. Convergence of the CCC results was demonstrated over the entire 10–300 eV energy range, and the calculation of the $b^3\Sigma_u^+$ ICS predicted a sharp peak at approximately 11.5 eV. The recommended data of Yoon *et al.* [9] are in substantial disagreement with the CCC results. Given the significance of the low-energy $b^3\Sigma_u^+$ excitation, it is important to determine an accurate cross section for this excitation process.

The FN approximation is not valid near excitation thresholds, where the vibrational motion of the nuclei has a significant effect. In this energy regime, the adiabatic nuclei (AN) approximation is a more accurate approach. The AN approximation has been previously applied to e^--H_2 excitation; for example, see the calculations by Trevisan and Tennyson [16], Celiberto *et al.* [17], and Rescigno and Schneider [18]. As with the FN calculations, these AN calculations are in significant disagreement with each other. The calculation of Trevisan and Tennyson [16] predicted a peak lower than both the Khakoo and Segura [7] and Nishimura and Danjo [6] measurements, and shifted to about 12.5 eV. The calculation of Celiberto *et al.* [17] was in reasonable agreement with the R-matrix calculation below 9 eV, but in substantial disagreement at higher energies, particularly in predicting a peak closer to 15 eV.

The success of the molecular CCC technique at above-threshold energies, and the need for accurate collision data over the entire range of impact energies for the excitation of the $b^3\Sigma_u^+$ state, motivates the present low-energy AN calculations. We also investigate the low-energy dissociation behavior of the H_2 isotopologues (D_2, T_2, HD, HT, and DT), which we expect will be important in tokamak fusion plasma modeling. It is worth noting that the AN CCC method was previously used to investigate positron collisions with H_2 [19] and electron collisions with H_2^+ [20,21], yielding good agreement with experiment.

*liam.scarlett@student.curtin.edu.au

II. THEORY

The molecular CCC method for e^--H_2 scattering has been described in detail in Refs. [15,21–23]. Here we give a brief overview. Atomic units are used throughout unless specified otherwise.

A. Molecular CCC method

The molecular CCC method utilizes the Born-Oppenheimer approximation to separate the electronic and nuclear degrees of freedom, allowing the electronic scattering problem to be solved in the FN approximation. The CCC method is formulated in the body frame, utilizing the spherical coordinate system, with the origin set at the midpoint between the two nuclei and the z axis aligned with the internuclear axis $\boldsymbol{R}$. In what follows, we suppress the explicit dependence on the internuclear separation R in the FN formulation of the CCC method and restore it later to make the presentation more transparent.

Molecular electronic target states are constructed by diagonalizing the target electronic Hamiltonian H_T in a basis of antisymmetrized two-electron configurations for each set of the conserved quantum numbers (m_t,π_t,s_t), where m_t is the total target angular momentum projection, s_t is the spin, and π_t is the parity:

$$\Phi_n^N(x_1,x_2) = \sum_{\alpha\beta} C_{\alpha\beta}^{(n)} \phi_\alpha(\boldsymbol{r}_1)\phi_\beta(\boldsymbol{r}_2)X(s_n,v_n), \tag{1}$$

where x_1 and x_2 are used to denote the spatial and spin coordinates of the electrons, and each n represents a set of the conserved quantum numbers. The coefficients $C_{\alpha\beta}^{(n)}$ are eigenvector components resulting from the diagonalization procedure and satisfy $C_{\alpha\beta}^{(n)} = (-1)^{s_n} C_{\beta\alpha}^{(n)}$ to ensure the antisymmetry of the two-electron configurations in Eq. (1). The spin function is given by

$$X(s,v) = \sum_{m_1 m_2} C^{sv}_{\frac{1}{2}m_1\frac{1}{2}m_2} \chi_{m_1}(\sigma_1)\chi_{m_2}(\sigma_2), \tag{2}$$

where $C^{lm}_{l_1 m_1 l_2 m_2}$ is a Clebsch-Gordan coefficient. The one-electron functions in Eq. (1) are given by

$$\phi_\alpha(\boldsymbol{r}) = \frac{1}{r}\varphi_{k_\alpha l_\alpha}(r) Y_{l_\alpha m_\alpha}(\hat{\boldsymbol{r}}), \tag{3}$$

where l is the angular momentum and φ_{kl} are the Laguerre basis functions,

$$\varphi_{kl}(r) = \sqrt{\frac{\alpha_l(k-1)!}{(k+l)(k+2l)!}}(2\alpha_l r)^{l+1} \times e^{-\alpha_l r} L_{k-1}^{2l+1}(2\alpha_l r), \quad k = 1,\ldots,N_l. \tag{4}$$

Here, α_l are the exponential fall-off parameters, L_{k-1}^{2l+1} are the associated Laguerre polynomials, and N_l is the number of functions for a given value of l. The resulting target pseudostates $\{\Phi_n^N\}_{n=1}^N$ satisfy

$$\left\langle \Phi_{n'}^N \middle| H_T \middle| \Phi_n^N \right\rangle = \varepsilon_n^N \delta_{n'n}, \tag{5}$$

where ε_n^N is the energy of the state Φ_n^N and N is the number of pseudostates.

The total scattering wave function is expressed as a multichannel expansion over the target states,

$$\Psi_i^{N(+)}(x_0,x_1,x_2) = \mathcal{A}\psi_i^{N(+)}(x_0,x_1,x_2) = \mathcal{A}\sum_{n=1}^{N} f_n^{N(+)}(x_0)\Phi_n^N(x_1,x_2), \tag{6}$$

where x_0 is the projectile spatial and spin coordinate, $(+)$ denotes outgoing spherical wave boundary conditions, $\mathcal{A} = 1 - P_{01} - P_{02}$ is the antisymmetrization operator, and P_{0i} is the space exchange operator.

Substituting the expansion (6) into the Schrödinger equation,

$$(E^{(+)} - H)\Psi_i^{N(+)} = 0, \tag{7}$$

results in a set of momentum-space Lippmann-Schwinger equations for the T matrix,

$$\left\langle \boldsymbol{k}_f^{(-)}\Phi_f^N \middle| T^N \middle| \Phi_i^N \boldsymbol{k}_i^{(+)} \right\rangle = \left\langle \boldsymbol{k}_f^{(-)}\Phi_f^N \middle| V \middle| \psi_i^{N(+)} \right\rangle, \tag{8}$$

where $|\boldsymbol{k}^{(\pm)}\rangle$ is a projectile distorted wave with energy $\varepsilon_k = k^2/2$.

The projectile wave function is expanded in partial waves,

$$|\boldsymbol{k}^{(\pm)}\rangle = \frac{1}{k}\sum_{L,M} i^L e^{\pm i\delta_L} Y_{LM}^*(\hat{\boldsymbol{k}})|kL\rangle, \tag{9}$$

where δ_L is the distorting phase shift and the sum is truncated at some $L_{\max}$. This allows a set of close-coupling equations to be formulated for the partial-wave T matrix. These equations are formed for each total symmetry specified by the total angular momentum projection M, parity Π, and spin S:

$$T^{M\Pi S}_{fL_fM_f,iL_iM_i}(k_f,k_i) = V^{M\Pi S}_{fL_fM_f,iL_iM_i}(k_f,k_i) + \sum_{n=1}^{N}\sum_{L'M'}\int_0^\infty dk \times \frac{V^{M\Pi S}_{fL_fM_f,nL'M'}(k_f,k)T^{M\Pi S}_{nL'M',iL_iM_i}(k,k_i)}{E^{(+)} - \varepsilon_k - \varepsilon_n^N + i0}, \tag{10}$$

and are solved by standard techniques [23,24].

The FN DCS analytically averaged over orientations is given by [15,23]

$$\frac{d\sigma_{f,i}^S(R,E_{\rm in})}{d\Omega} = \sum_j D_{f,i}^{Sj} P_j(\cos\theta), \tag{11}$$

where P_j is the Legendre polynomial and the DCS coefficients are

$$D_{f,i}^{Sj} = \pi^2 \frac{q_f(R;E_{\rm in})}{q_i}\sum_{\substack{M,\Pi\\M',\Pi'}}\sum_{\substack{L_f,L_i\\M_f,M_i}}\sum_{\substack{L'_f,L'_i\\M'_f,M'_i}} i^{L_i-L_f+L'_i-L'_f} \times (-1)^{M'_f+M'_i}\hat{L}_i\hat{L}'_i\hat{L}_f\hat{L}'_f(2j+1)^{-1} \times T^{M\Pi S}_{fL_fM_f,iL_iM_i}(R,E_{\rm in})T^{M'\Pi' S*}_{fL'_fM'_f,iL'_iM'_i}(R,E_{\rm in}) \times C^{j0}_{L_i0,L'_i0}C^{jM'_i-M_i}_{L_i-M_i,L'_iM'_i}C^{jM_f-M'_f}_{L_fM_f,L'_f-M'_f} \times C^{j0}_{L_f0,L'_f0}\delta_{M_i-M'_i,M_f-M'_f}. \tag{12}$$

Here, $\hat{L} = \sqrt{2L+1}$, and q_f, q_i are the outgoing and incident projectile momenta, respectively:

$$q_f(R;E_{\rm in}) = \sqrt{2[E_{\rm in} - \varepsilon_{f,i}(R)]}, \tag{13}$$

$$q_i = \sqrt{2E_{\rm in}}. \tag{14}$$

Note that q_f depends only on the incident energy $E_{\rm in}$ and the electronic excitation energy $\varepsilon_{f,i}(R) = \varepsilon_f(R) - \varepsilon_i(R)$. The on-shell physical FN T matrix $T^{M\Pi S}_{fL_fM_f,iL_iM_i}(R;E_{\rm in})$ in Eq. (12) is obtained from the solution of the Lippmann-Schwinger equations (10) [22], where we have restored the explicit R dependence.

The FN ICS $\sigma^S_{f,i}$ are obtained by integrating Eq. (11). As a result of the orthogonality property of the Legendre polynomials, only the $j = 0$ term of the summation is nonzero after integration over solid angle, which gives

$$\sigma^S_{f,i}(R;E_{\rm in}) = \int \frac{d\sigma^S_{f,i}}{d\Omega} d\Omega = 4\pi D^{S0}_{f,i} = 4\pi^3 \frac{q_f(R;E_{\rm in})}{q_i} \sum_{\substack{M,\Pi \\ L_f,L_i \\ M_f,M_i}} \left| T^{M\Pi S}_{fL_fM_f,iL_iM_i}(R;E_{\rm in}) \right|^2. \tag{15}$$

B. Adiabatic nuclei method

Bound target vibrational wave functions $\chi_{nv_n}(R)$ are obtained by diagonalizing the Born-Oppenheimer Hamiltonian,

$$\mathcal{H} = -\frac{1}{2\mu}\frac{d^2}{dR^2} + \frac{J(J+1) - m_n^2}{2\mu R^2} + \varepsilon_n(R), \tag{16}$$

in a basis of nuclear functions which have the same form as the one-electron functions (3). Here, μ is the reduced mass of the molecule (calculated for each isotopologue using 1836.15, 3670.48, and 5496.92 for the proton, deuteron, and triton mass, respectively), J is the rotational quantum number, m_n is the angular momentum projection, and $\varepsilon_n(R)$ is the potential-energy function for the electronic state Φ^N_n. At present, we remove the rotational dependence of the vibrational wave functions by setting $J = 0$. Note that vibrational wave functions depend only weakly on J since the rotational term of Eq. (16) is of the order of $1/\mu \approx 10^{-3}$ and is therefore negligible compared to the potential-energy term. The basis size is chosen to yield convergent bound-state solutions of the Schrödinger equation,

$$\langle \chi_{nv'_n} | \mathcal{H} | \chi_{nv_n} \rangle = \epsilon_{v_n} \delta_{v'_n v_n}, \tag{17}$$

where ϵ_{v_n} is the energy of the bound vibrational wave function χ_{nv_n}. The vibrational wave functions satisfy the following closure property:

$$\sum\!\!\!\!\!\!\int_{v_n} \chi_{nv_n}(R)\chi_{nv_n}(R') = \delta(R - R'), \tag{18}$$

where the summation is over the discrete spectrum and the integration is over the continuum.

Following the AN approximation [25], the ICS $\sigma^S_{fv_f,iv_i}$ and DCS $d\sigma^S_{fv_f,iv_i}/d\Omega$ for the vibrationally resolved transition $iv_i \to fv_f$ are obtained via the substitution

$$\sqrt{q_f(R_{\rm m};E_{\rm in})}\, T^{M\Pi S}_{fL_fM_f,iL_iM_i}(R_{\rm m};E_{\rm in}) \to \langle \chi_{fv_f} | \sqrt{q_f(R;E_{\rm in})}\, T^{M\Pi S}_{fL_fM_f,iL_iM_i}(R;E_{\rm in}) | \chi_{iv_i} \rangle \tag{19}$$

in Eqs. (11), (12), and (15). To obtain the AN T matrix, one has to conduct FN calculations at many internuclear distances in order to perform accurate integration over R in Eq. (19).

The closure property (18) is used to obtain cross sections summed over all final bound vibrational states and integrated over all final vibrational continuum states, yielding

$$\frac{d\sigma^S_{f,iv_i}}{d\Omega} = \sum\!\!\!\!\!\!\int_{v_f} \frac{d\sigma^S_{fv_f,iv_i}}{d\Omega} = \langle \chi_{iv_i} | \frac{d\sigma^S_{f,i}}{d\Omega} | \chi_{i,v_i} \rangle. \tag{20}$$

Note that this technique requires the outgoing electron momentum and FN T matrix in Eq. (19) to be independent of the final vibrational state energy. This condition is satisfied due to the definition of q_f in Eq. (13). Closure relations have been previously utilized to sum cross sections over final rovibrational states, in the Born approximation in Refs. [26–28], and in the CCC method by Zammit *et al.* [19,22] and Scarlett *et al.* [20].

Spin-averaged cross sections are obtained using

$$\frac{d\sigma_{f,iv_i}}{d\Omega} = \sum_S \frac{2S+1}{2(2s_i+1)} \frac{d\sigma^S_{f,iv_i}}{d\Omega}, \tag{21}$$

where s_i is the initial target state spin. The same expressions (20) and (21) hold for the ICS. For scattering on the ground state of H_2, $s_i = 0$ and hence there is only one spin channel. Furthermore, in this paper, we consider only scattering from the ground vibrational level ($v_i = 0$).

The problem of energy conservation in the AN approximation has been discussed previously for vibrational excitations by Mazevet *et al.* [29] and for electronic excitations by Shugard and Hazi [30] and Ficocelli Varracchio [31]. There is a discrepancy between the true excitation energy and the FN electronic excitation energy, which does not consider the vibrational levels. For scattering on the ground vibrational state, the error in the initial state energy is relatively small over the extent of the $v = 0$ wave function, but as the integrand in Eq. (19) varies with R, the error in the final state energy can be much larger, except at the classical turning point(s) of the final state wave function. The corrections suggested by Shugard and Hazi [30] and Ficocelli Varracchio [31] both require the use of off-shell T-matrix elements. Stibbe and Tennyson [32] suggested an energy-balancing method for the $b^3\Sigma^+_u$ AN cross section which fixes the outgoing electron energy at the correct value for a given fragment kinetic energy, but varies the incident energy over R to allow the use of T matrices which are on the energy shell in the FN formalism. It is not clear how significant the benefits of the energy-balancing method [32] are since, without the use of off-shell FN T matrices, the violation of energy conservation is unavoidable. Because of the larger number of calculations required to perform accurate interpolation over both energy and R for the energy-balancing method, here we apply the standard AN method as detailed in the review of Lane [25]. This method has been applied to dissociative processes in a number of

previous works [20,26–28,33,34], yielding results in good agreement with experiment. Peek and Green [35,36] showed that the standard AN method is sufficiently accurate for the dissociative $1s\sigma_g \rightarrow 2p\sigma_u$ transition in H_2^+ at intermediate to high energies.

III. METHODOLOGY

In the previous FN CCC calculations of e^--H_2 scattering [15], we have conducted detailed convergence studies for the $b^3\Sigma_u^+$ excitation. We found that for incident electron energies below 12 eV, the close-coupling calculations that include nine states are in good agreement with calculations that include a larger number of states in the close-coupling expansion (up to the maximum of 491 states). Since the effect of interchannel coupling is weaker at low energies and because the AN approach requires a large number of calculations at many internuclear distances, here we have performed AN calculations with a model that includes the following 12 states: $X^1\Sigma_g^+$, $b^3\Sigma_u^+$, $a^3\Sigma_g^+$, $c^3\Pi_u$, $B^1\Sigma_u^+$, $E,F^1\Sigma_g^+$, $C^1\Pi_u$, $B'^1\Sigma_u^+$, and $D^1\Pi_u$. Note that Π states enter the close-coupling expansion twice (for $m_t = +1$ and $m_t = -1$). We have reserved the notation CCC for models that account for coupling to ionization channels and CC for the models that include only the electronic bound states. In addition to the AN calculations performed with the CC(12) model, we have also conducted AN calculations with the CC(48) model to verify the convergence of the AN $b^3\Sigma_u^+$ cross sections. The latter model contains the first 48 states for $R = 1.448$. The target wave functions for the CC(12) and CC(48) models have been obtained with the same one-electron basis and set of two-electron configurations as described in Ref. [15] for the CCC(491) model.

Each model utilized the same underlying description of the H_2 wave functions. The one-electron functions (3) were constructed from a Laguerre basis including $N_l = 17 - l$ functions up to $l_{max} = 3$, with exponential falloffs ranging from 0.76 to 0.85. The $1s\sigma_g$ one-electron orbital was constructed using $N_l = 60 - l$ functions up to $l_{max} = 8$, with $\alpha_l = 0.9$. The CC(12) scattering calculations were performed using a projectile partial-wave expansion up to $L_{max} = 6$, including all total angular momentum projection M, even and odd parity Π, and total spin $S = 1/2$ channels up to $M_{max} = 6$. Each CC(12) calculation at a fixed energy and internuclear separation required approximately six hours of CPU time, distributed over 24 parallel threads on a 12-core Haswell processor. For the CC(48) model, we took $L_{max} = M_{max} = 5$, with each calculation requiring approximately 60 hours, distributed over 120 parallel threads on five processors. We find that for triplet state excitations, the partial-wave convergence is readily established with $M_{max} = 5$, not only at the low energies considered in this work, but across all energies [15]. This has also been observed in the R-matrix calculations of Trevisan and Tennyson [16].

Calculations were performed over a range of internuclear separations up to $R = 2.5$ and energies up to 14 eV. At a given incident energy, the R-dependent ICS exhibit complex resonance structures which shift towards lower R at higher incident energies. To minimize the number of calculations required, we utilized a relatively coarse R mesh (steps of 0.1) in regions where the cross section is smooth, but used a much finer mesh (steps of 0.01) around the resonances to ensure the accuracy of the AN calculations.

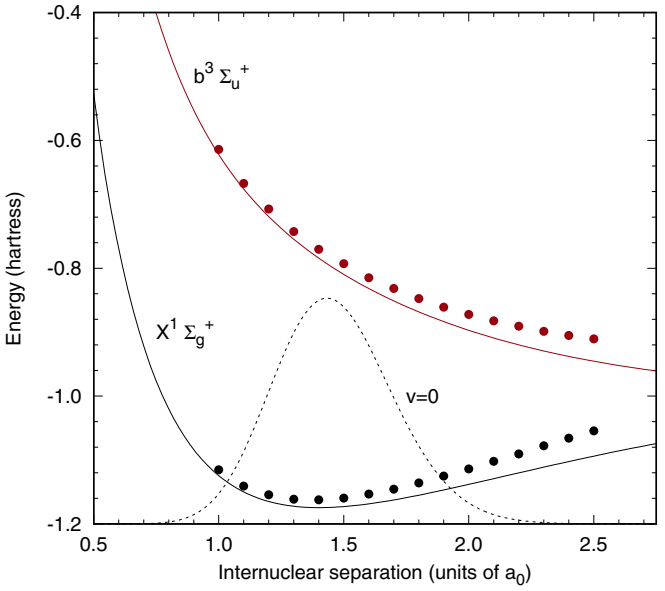

FIG. 1. Potential-energy curves of the $X^1\Sigma_g^+$ and $b^3\Sigma_u^+$ states of H_2 obtained from structure calculations performed in the present scattering calculation model (points), compared with the accurate calculations (solid lines) of Kolos *et al.* [37] ($X^1\Sigma_g^+$) and Staszewska and Wolniewicz [38] ($b^3\Sigma_u^+$). The ground (electronic and vibrational) wave function of H_2 is also shown (dashed line).

IV. RESULTS

In Fig. 1, we present the potential energy curves (PEC) of the $X^1\Sigma_g^+$ and $b^3\Sigma_u^+$ states obtained using the present (single-center spherical coordinate) structure model and compare with the accurate calculations of Kolos *et al.* [37] ($X^1\Sigma_g^+$) and Staszewska and Wolniewicz [38] ($b^3\Sigma_u^+$). On the same figure, we have also presented the ground-state ($v = 0$) vibrational wave function of H_2. We find that the present structure model is sufficiently accurate to perform scattering calculations over the range of R points at which the $v = 0$ vibrational wave function is nonzero (below 2.3). To improve the accuracy of the AN CCC cross sections, we have obtained the vibrational wave functions using the accurate PEC of Kolos *et al.* [37].

A. Convergence studies

AN calculations of electron-impact excitation of the $b^3\Sigma_u^+$ state of H_2 have been performed in the range of incident energies from 6 to 14 eV. In Fig. 2, we present the AN CC(12) $b^3\Sigma_u^+$ cross sections and compare with a number of AN CC(48) calculations to demonstrate convergence. We also compare the AN results with the CC(12) and CCC(491) FN cross sections performed at $R = 1.448$. The FN CC(12) results have prominent resonance structures near 12 eV. The same resonance structures were observed in the calculations of Branchett *et al.* [12] and Trevisan and Tennyson [16]. The previous FN CCC(491) calculations were performed over a 1 eV mesh (at these low energies), and no attempts were made

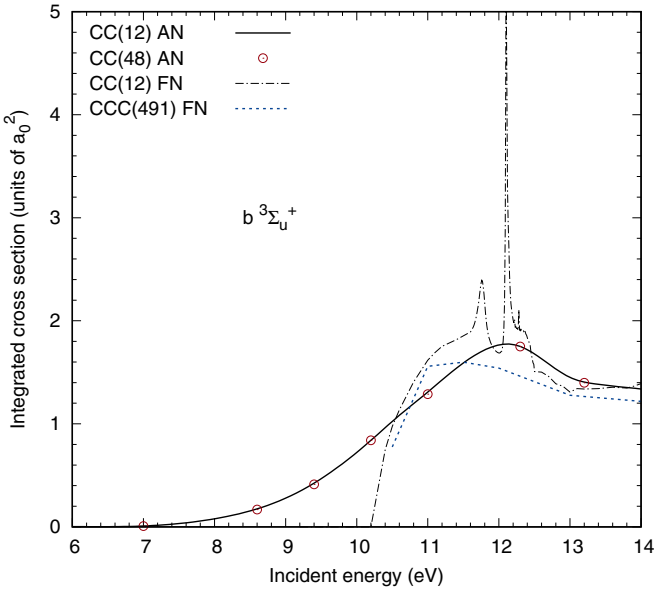

FIG. 2. Electron-impact excitation cross section of the $b^3\Sigma_u^+$ state of H_2. Convergence is demonstrated for the AN CC(12) and CC(48) models described in the text. The FN CCC(491) and CC(12) calculations performed at $R = 1.448$ are also presented.

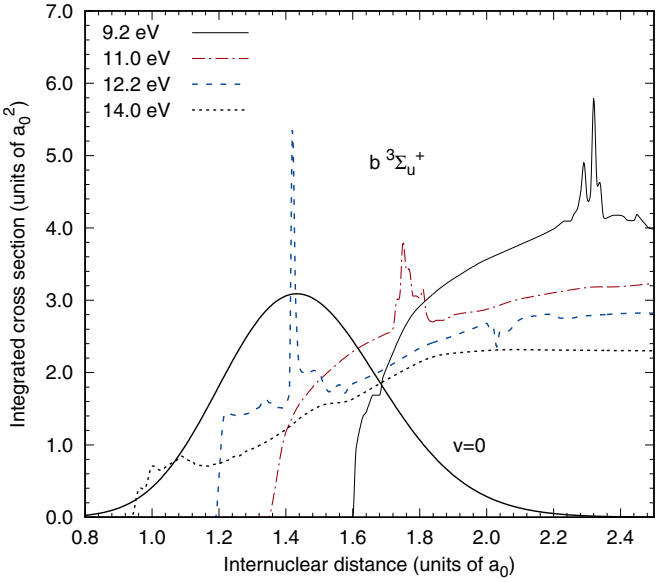

FIG. 3. The R-dependent electron-impact excitation cross section of the $b^3\Sigma_u^+$ state of H_2 at $E_{in} = 9.2$, 11.0, 12.2, and 14.0 eV, demonstrating the shifting of the resonances and excitation thresholds towards lower R as E_{in} is increased. The ground (electronic and vibrational) state wave function of H_2 is also shown.

to map out resonances because it was expected that they will be averaged over in the AN calculations, as indeed can be seen from Fig. 2.

B. Comparison of adiabatic and fixed-nuclei methods

Figure 2 shows that the CC(12) AN and FN cross sections are in reasonable agreement by 14 eV. We therefore expect that the vibrational motion effects become insignificant above this energy, and hence the FN results are sufficient. In Fig. 3, we present the R-dependent $b^3\Sigma_u^+$ ICS at 9.2, 11.0, 12.2, and 14.0 eV incident energies, obtained from FN calculations performed at a large number of R points. At a given incident electron energy, the AN cross section is best approximated by the FN cross section when the threshold of the R-dependent ICS $\sigma_{f,i}(R)$ is much lower than the bond length $R = 1.4$. As detailed by Zhang and Mitroy [39], expanding the R-dependent ICS via a Taylor series about some $R = R_0$ gives the AN cross section in the following form:

$$\sigma_{f,iv_i} = \sigma_{f,i}(R_0) + \left(\frac{d\sigma_{f,i}}{dR}\right)_{R_0} \langle \chi_{iv_i} | (R - R_0) | \chi_{iv_i} \rangle + \cdots . \tag{22}$$

The error is minimized by choosing $R_0 = R_m = 1.448$, the mean internuclear separation of the $v = 0$ vibrational wave function, since the second term of Eq. (22) vanishes. At low energies, where the threshold of the R-dependent ICS is near the bond length, the expansion about R_m is dominated by higher-order terms and the FN approximation becomes invalid. At higher energies, if the R-dependent ICS can be approximated by a straight line over the extent of the wave function, then the FN approximation becomes accurate as higher-order terms vanish. This is indeed the case for the 14 eV cross section. Interestingly, Fig. 3 also shows that the resonances in the R-dependent ICS shift towards lower R as the incident energy is increased.

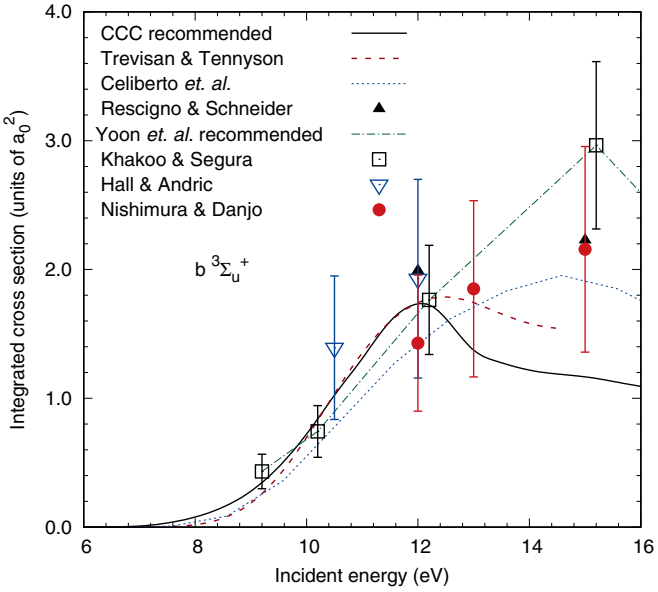

FIG. 4. Electron-impact excitation cross section of the $b^3\Sigma_u^+$ state of H_2. The recommended CCC cross section is compared with the calculations of Trevisan and Tennyson [16], Celiberto *et al.* [17], and Rescigno and Schneider [18], the measurements of Khakoo and Segura [7], Nishimura and Danjo [6], and Hall and Andric [8], and the recommended data of Yoon *et al.* [9].

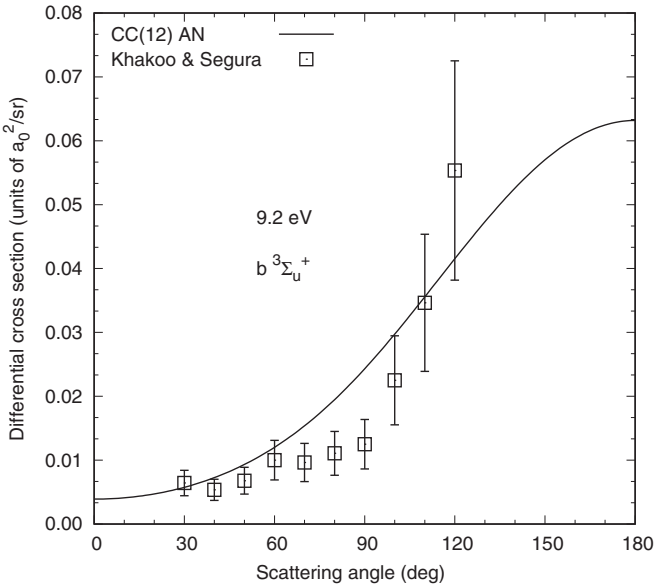

FIG. 5. Electron-impact differential excitation cross section of the $b^3\Sigma_u^+$ state of H_2 at 9.2 eV, calculated with the AN CC(12) model described in the text, and compared with the experiment of Khakoo and Segura [7].

C. Integrated cross sections

The CC(12) model is not expected to be valid at incident energies above approximately 12 eV, as demonstrated by the disagreement between the CC(12) and CCC(491) FN results at higher energies (see Ref. [15] for convergence studies of several FN CCC models). To produce a recommended CCC cross section, we use the AN CC(12) results up to 11.5 eV and the FN CCC(491) results above 14 eV. In the 11.5–14 eV energy interval, we take an average of the CC(12) and CCC(491) results, using a weight function which varies linearly between 11.5 and 14 eV in order to smoothly connect the two cross sections. These results are presented in Fig. 4 and compared with the AN R-matrix calculations of Trevisan and Tennyson [16], the AN semiclassical calculations of Celiberto *et al.* [17], the AN complex Kohn calculations of Rescigno and Schneider [18], the measurements of Khakoo and Segura [7], Nishimura and Danjo [6], and Hall and Andric [8], and the recommended data of Yoon *et al.* [9]. The CCC calculations are in good agreement with all three measurements below approximately 12.5 eV. The CCC and R-matrix results are in good agreement between 10 and 12 eV and both methods suggest a smaller peak shifted to lower energies compared to what was found in experiment. As the CCC and R-matrix calculations utilize a similar close-coupling expansion, the small discrepancy between the two methods below 10 eV is likely due to the use of the energy-correction method in the R-matrix calculation, which is expected to have the greatest effect at energies close to threshold. The present results, however, are in better agreement with the measurements of Khakoo and Segura [7] in this region. Clearly, the techniques for dealing with energy conservation in the AN method deserve further investigation.

Above 12 eV, the present results are lower than the R-matrix results. This is to be expected since the R-matrix calculation included fewer states in the close-coupling expansion, in the same way that the CC(12) model produced a larger FN cross section than the CCC(491) model at these energies. The calculation of Celiberto *et al.* [17] is in good agreement with the measurements of Nishimura and Danjo [6] and passes through or just below the lower error bounds of Khakoo and Segura [7] and Hall and Andric [8]. The peak predicted by Celiberto *et al.* [17] is significantly lower than the recommended data [9], which follows the peak of Khakoo and Segura [7]. The Celiberto *et al.* [17] results are semiclassical and are not expected to be correct at low energies. Despite the differences between the three calculations, they all predict a cross section substantially lower than the recommended data around 15 eV. This qualitative agreement between all three theoretical methods indicates that the experiments have likely overestimated the true cross section. This is unlikely due to cascades from higher triplet states as the ICS were obtained by integrating over DCS measurements, which were obtained by measuring the electron energy-loss spectrum. At 15 eV, the energy-loss spectra for the higher states overlap the $b^3\Sigma_u^+$ spectrum by approximately 20% [7], which cannot account for the large difference between the theory and experiments. The accuracy of the CCC $b^3\Sigma_u^+$ cross section is supported by the excellent agreement of the CCC total cross section with experiment [15]. The calculations of Rescigno and Schneider [18] were performed at just a few energies, with no calculations performed below 12 eV. These calculations predicted a peak near 15 eV, in disagreement with the present results and the calculations of Trevisan and Tennyson [16].

D. Differential cross sections

In Fig. 5, we present the $b^3\Sigma_u^+$ DCS at $E_{\rm in} = 9.2$ eV, compared with the measurements of Khakoo and Segura [7]. The CCC calculations were not previously available at 9.2 eV [15] since the $b^3\Sigma_u^+$ excitation is closed in the FN model at this

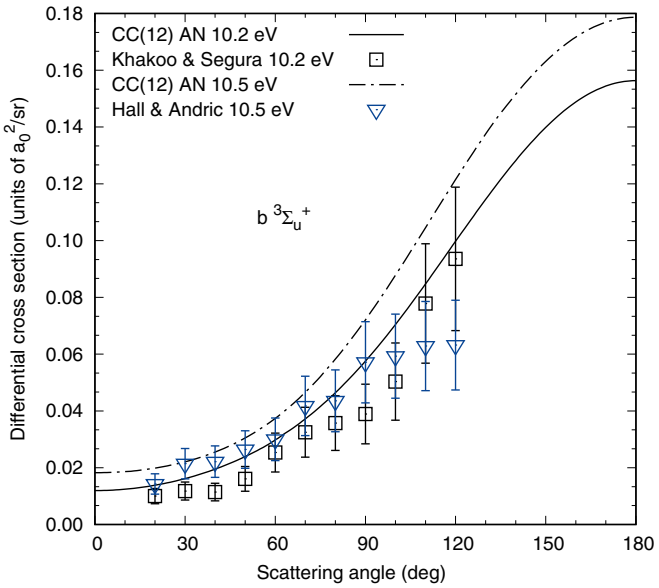

FIG. 6. Same as in Fig. 5, but at 10.2 and 10.5 eV, and including the measurements of Hall and Andric [8].

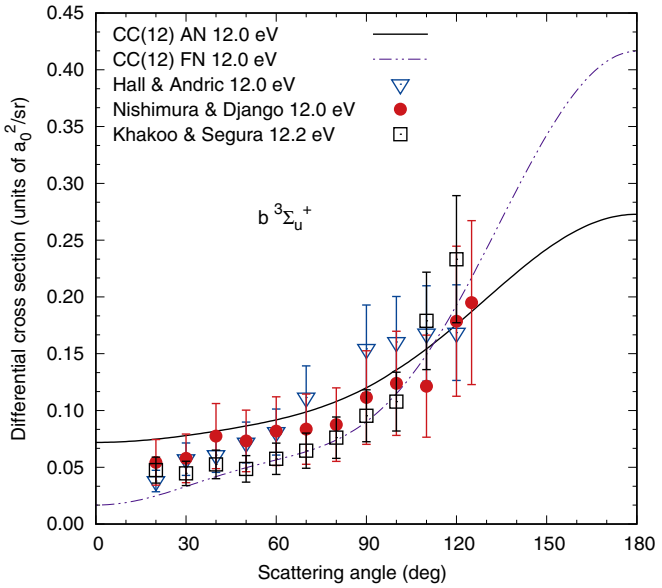

FIG. 7. Same as in Fig. 6, but at 12 eV, and including the measurements of Nishimura and Danjo [6]. Also shown is the CC(12) FN calculation described in the text.

energy. The low-energy $b^3\Sigma_u^+$ DCS were also calculated by Trevisan and Tennyson [16] using the AN R-matrix method; however, they were affected by an error in the accounting of phase factors [40] and hence we exclude them here and in the remaining DCS figures.

In Fig. 6, we present the $b^3\Sigma_u^+$ DCS at incident energies of 10.2 and 10.5 eV. We compare with the measurements of Khakoo and Segura [7] (10.2 eV) and Hall and Andric [8] (10.5 eV). The CCC 10.2 eV DCS is in good agreement with the Khakoo and Segura [7] measurements. The measurements of Hall and Andric [8] show a flattening of the DCS between 90 and 120 degrees, while the Khakoo and Segura [7] experiment shows a sharp rise in the same region. Although the present 10.5 eV results and the measurements of Hall and Andric [8] are in agreement up to 90 degrees, they do not agree at backwards scattering angles.

In Fig. 7, we present the $b^3\Sigma_u^+$ DCS at $E_{\rm in} = 12$ eV. We compare with the measurements of Khakoo and Segura [7] (12.2 eV), Nishimura and Danjo [6] (12 eV), and Hall and Andric [8] (12 eV). At this energy, we expect the vibrational motion effects are still important, which is illustrated by the quantitative and qualitative differences between the AN and FN results. While the CC(12) FN DCS is in good agreement with the measurements of Khakoo and Segura [7], the CC(12) AN DCS is in good agreement with the Nishimura and Danjo [6] measurements, and with the Hall and Andric [8] measurements above 50 degrees. The 12 eV DCS here and in the following section for the isotopologues have been scaled down by approximately 2% to be consistent with the recommended CCC AN ICS, which was scaled down above 11.5 eV to connect to the CCC(491) results.

Performing the AN calculations results in a flatter DCS than is seen in the FN ($R = 1.448$) results. This is a result of the flatter FN DCS at R values to either side of $R = 1.448$, within the range which makes the most significant contribution to the AN DCS. At backwards scattering angles, the measurements of Hall and Andric [8] appear flatter than both the present calculations and the two other measurements. Given the relatively large error bars at these angles, however, this is not particularly significant.

E. The isotope effect

In the present CCC formulation, the electronic and nuclear degrees of freedom are separated using the Born-Oppenheimer approximation, and hence the electronic structure and FN

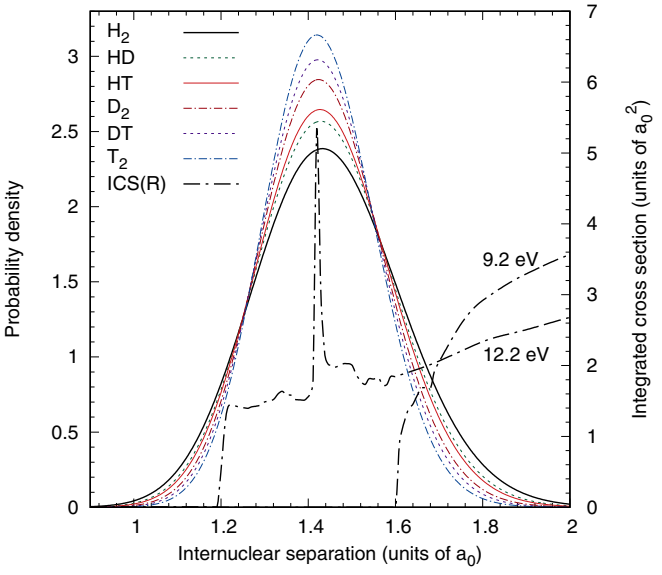

FIG. 8. Probability density functions of the ground vibrational state for H_2 and its isotopologues. The R-dependent excitation cross sections of the $b^3\Sigma_u^+$ state at 9.2 and 12.2 eV are also shown.

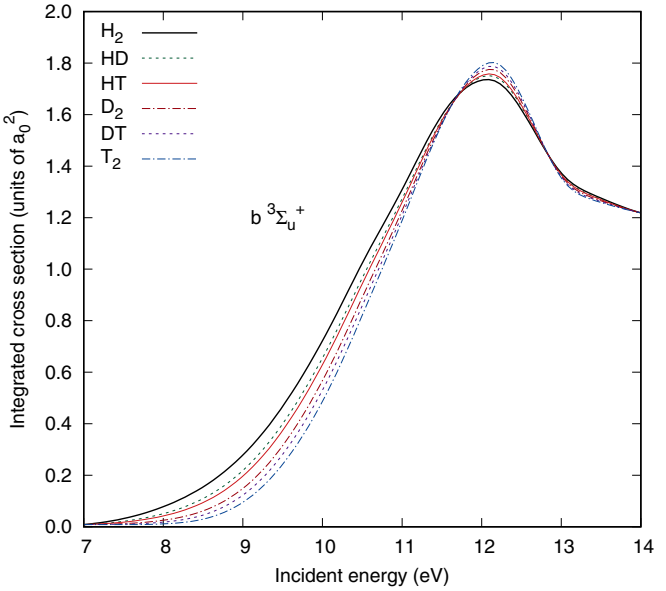

FIG. 9. Electron-impact excitation cross section of the $b^3\Sigma_u^+$ state of H_2, D_2, T_2, HD, HT, and DT, calculated using the AN CC(12) model described in the text.

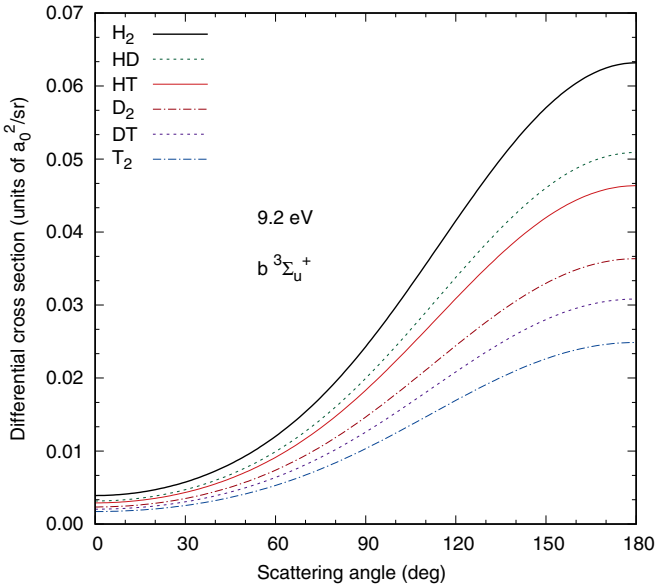

FIG. 10. Electron-impact differential excitation cross sections of the $b^3\Sigma_u^+$ state of H_2, D_2, T_2, HD, HT, and DT at 9.2 eV, calculated using the AN CC(12) model described in the text.

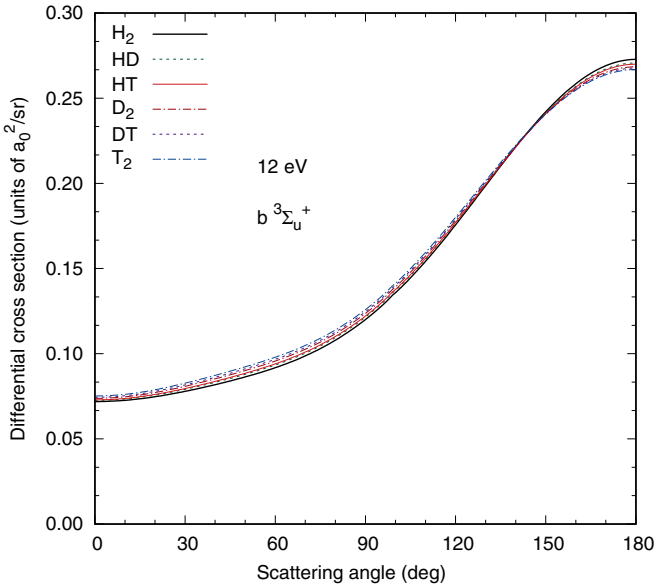

FIG. 12. Same as in Fig. 10 but at 12 eV.

collision data are identical among the isotopologues H_2, D_2, T_2, HD, HT, and DT. However, the AN cross sections differ for the isotopologues due to the difference in the ground-state vibrational wave function. The increased reduced mass of the heavier isotopologues causes the ground-state vibrational wave function to become contracted and display a larger probability density near the mean internuclear separation (see Fig. 8). At low energies, the excitation threshold of the R-dependent cross section shifts to larger R, and hence the smaller probability density of the vibrational wave function at larger R for the heavier isotopologues leads to a reduced AN cross section. This is illustrated in Fig. 8 by the R-dependent ICS at 9.2 eV. At larger energies, such as 12.2 eV, the excitation threshold shifts to lower R and the isotope effect is less pronounced.

In Fig. 9, we compare the recommended CCC AN ICS for the isotopologues of H_2. These have been constructed in the same manner as the H_2 ICS in Fig. 4. There is a strong isotope effect at incident energies up to approximately 11.5 eV, above which there are minor differences between the different species.

In Figs. 10–12, we compare the DCS for the isotopologues of H_2 at $E_{in} = 9.2$, 10.2, and 12 eV, respectively. As for the ICS, the isotope effect is stronger at lower incident electron energies. The 9.2 and 10.2 eV DCS are decreased significantly at backwards scattering angles for the heavier isotopologues, leading to a flattening of the overall DCS. At $E_{in} = 12$ eV, there are no significant differences in the DCS for the different species.

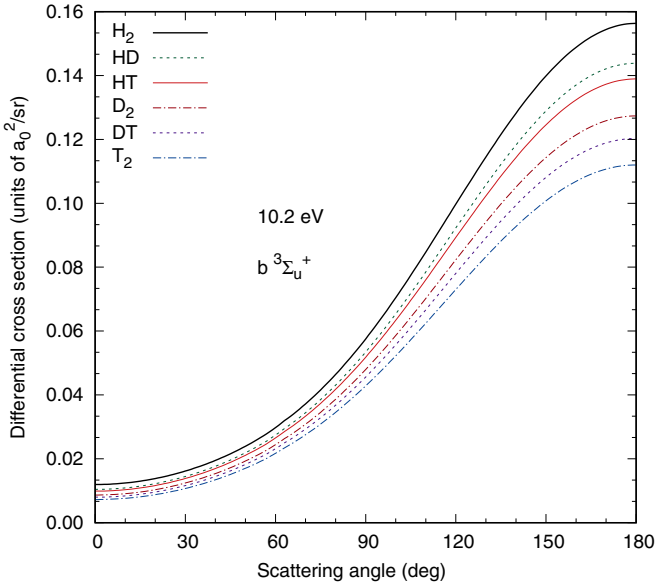

FIG. 11. Same as in Fig. 10, but at 10.2 eV.

V. CONCLUSIONS

We have calculated integrated and differential cross sections for low-energy electron-impact excitation of the $b^3\Sigma_u^+$ state of H_2 and its isotopologues in the AN approximation. Below 12 eV, our ICS results are in good agreement with the measurements of Khakoo and Segura [7] and Hall and Andric [8], and with the previous AN R-matrix calculations of Trevisan and Tennyson [16], but are somewhat larger than the semiclassical calculations of Celiberto *et al.* [17]. Above approximately 12.5 eV, the present results are substantially lower than both the semiclassical [17] and R-matrix [16] calculations, and all three calculations are systematically lower than the recommended data of Yoon *et al.* [9] in this region. The discrepancy between the three calculations and the recommended data deserves further investigation. For the DCS, we have produced a set of theoretical $b^3\Sigma_u^+$ cross sections that are in good agreement with the available experiments in the low-energy regime from 9.2 to 12 eV.

We have shown that the ICS and DCS are highly sensitive to the isotope effect at energies below 12 eV, and expect that this can be of importance for modeling low-temperature plasmas containing these species. Above 13 eV, the AN calculations are in reasonable agreement with the corresponding FN results and, therefore, the much computationally cheaper FN approach is sufficiently accurate. The reasons for the disagreement between the AN and FN results at low energies, and agreement at high energies have been discussed and explained. We have presented our recommended ICS, which connect the present AN results to the previously published [15] CCC FN results.

The theoretical techniques utilized in the present work can be extended to low-energy excitations of excited electronic states, scattering from hot (vibrationally excited) targets, and calculations of fully vibrationally resolved excitations. If the energy of the scattered electron is comparable to the vibrational level spacings, a fully quantum mechanical treatment of the nuclear motion, such as vibrational close coupling, may be required. However, the present techniques are likely to be sufficiently accurate at energies of interest in plasma modeling applications.

ACKNOWLEDGMENTS

This work was supported by the United States Air Force Office of Scientific Research, Los Alamos National Laboratory (LANL), Curtin University, and resources provided by the Pawsey Supercomputing Centre, with funding from the Australian Government and Government of Western Australia. M.C.Z. would like to specifically acknowledge LANL's ASC PEM Atomic Physics Project for its support. LANL is operated by Los Alamos National Security, LLC for the National Nuclear Security Administration of the U.S. Department of Energy under Contract No. DE-AC52- 06NA25396.

[1] C. Jonin, X. Liu, J. M. Ajello, G. K. James, and H. Abgrall, Astrophys. J. Suppl. Ser. **129**, 247 (2000).
[2] X. Liu, S. M. Ahmed, R. A. Multari, G. K. James, and J. M. Ajello, Astrophys. J. Suppl. Ser. **101**, 375 (1995).
[3] D.-H. Ki and Y.-D. Jung, Astrophys. J. Suppl. Ser. **204**, 18 (2013).
[4] K. Sawada and T. Fujimoto, J. Appl. Phys. **78**, 2913 (1995).
[5] S. J. B. Corrigan, J. Chem. Phys. **43**, 4381 (1965).
[6] H. Nishimura and A. Danjo, J. Phys. Soc. Jpn. **55**, 3031 (1986).
[7] M. A. Khakoo and J. Segura, J. Phys. B At. Mol. Opt. Phys. **27**, 2355 (1994).
[8] R. I. Hall and L. Andric, J. Phys. B At. Mol. Phys. **17**, 3815 (1984).
[9] J.-S. Yoon, M.-Y. Song, J.-M. Han, S. H. Hwang, W.-S. Chang, B. Lee, and Y. Itikawa, J. Phys. Chem. Ref. Data **37**, 913 (2008).
[10] B. I. Schneider and L. A. Collins, J. Phys. B At. Mol. Phys. **18**, L857 (1985).
[11] R. F. da Costa, F. J. da Paixão, and M. A. P. Lima, J. Phys. B At. Mol. Opt. Phys. **38**, 4363 (2005).
[12] S. E. Branchett, J. Tennyson, and L. A. Morgan, J. Phys. B At. Mol. Opt. Phys. **23**, 4625 (1990).
[13] J. D. Gorfinkiel and J. Tennyson, J. Phys. B **38**, 1607 (2005).
[14] A. W. Fliflet and V. McKoy, Phys. Rev. A **21**, 1863 (1980).
[15] M. C. Zammit, J. S. Savage, D. V. Fursa, and I. Bray, Phys. Rev. A **95**, 022708 (2017).
[16] C. S. Trevisan and J. Tennyson, J. Phys. B At. Mol. Opt. Phys. **34**, 2935 (2001).
[17] R. Celiberto, R. Jenev, A. Laricchiuta, M. Capitelli, J. Wadehra, and D. Atems, At. Data Nucl. Data Tables **77**, 161 (2001).
[18] T. N. Rescigno and B. I. Schneider, J. Phys. B At. Mol. Phys. **21**, L691 (1988).
[19] M. C. Zammit, D. V. Fursa, J. S. Savage, L. Chiari, A. Zecca, and M. J. Brunger, Phys. Rev. A **95**, 022707 (2017).
[20] L. H. Scarlett, M. C. Zammit, D. V. Fursa, and I. Bray, Phys. Rev. A **96**, 022706 (2017).
[21] M. C. Zammit, D. V. Fursa, and I. Bray, Phys. Rev. A **90**, 022711 (2014).
[22] M. C. Zammit, D. V. Fursa, and I. Bray, Phys. Rev. A **88**, 062709 (2013).
[23] M. C. Zammit, D. V. Fursa, J. S. Savage, and I. Bray, J. Phys. B At. Mol. Opt. Phys. **50**, 123001 (2017).
[24] I. Bray and A. T. Stelbovics, Phys. Rev. A **46**, 6995 (1992).
[25] N. F. Lane, Rev. Mod. Phys. **52**, 29 (1980).
[26] J. M. Peek, Phys. Rev. **140**, A11 (1965).
[27] J. M. Peek, Phys. Rev. **154**, 52 (1967).
[28] J. M. Peek, Phys. Rev. A **10**, 539 (1974).
[29] S. Mazevet, M. A. Morrison, O. Boydstun, and R. K. Nesbet, J. Phys. B At. Mol. Opt. Phys. **32**, 1269 (1999).
[30] M. Shugard and A. U. Hazi, Phys. Rev. A **12**, 1895 (1975).
[31] E. F. Varracchio, J. Phys. B At. Mol. Phys. **14**, L511 (1981).
[32] D. T. Stibbe and J. Tennyson, New J. Phys. **1**, 2 (1998).
[33] J. M. Peek, Phys. Rev. **134**, A877 (1964).
[34] T. A. Green and J. M. Peek, Phys. Rev. **183**, 166 (1969).
[35] J. M. Peek, Phys. Rev. **183**, 193 (1969).
[36] J. M. Peek and T. A. Green, Phys. Rev. **183**, 202 (1969).
[37] W. Kolos, K. Szalewicz, and H. J. Monkhorst, J. Chem. Phys. **84**, 3278 (1986).
[38] G. Staszewska and L. Wolniewicz, J. Mol. Spectrosc. **198**, 416 (1999).
[39] J. Y. Zhang and J. Mitroy, Phys. Rev. A **83**, 022711 (2011).
[40] J. Tennyson, Comp. Phys. Comm. **100**, 26 (1997).